Venus Observations at 40 and 90 GHz with CLASS

Sumit Dahal [ID],[1,2] Michael K. Brewer,[2] John W. Appel [ID],[2] Aamir Ali [ID],[3,2] Charles L. Bennett [ID],[2]
Ricardo Bustos [ID],[4] Manwei Chan,[2] David T. Chuss [ID],[5] Joseph Cleary,[2] Jullianna D. Couto [ID],[2]
Rahul Datta [ID],[2] Kevin L. Denis,[1] Joseph Eimer [ID],[2] Francisco Espinoza,[4] Thomas Essinger-Hileman [ID],[1,2]
Dominik Gothe,[2] Kathleen Harrington [ID],[6,2] Jeffrey Iuliano [ID],[2] John Karakla,[2] Tobias A. Marriage [ID],[2]
Sasha Novack,[2] Carolina Núñez [ID],[2] Ivan L. Padilla [ID],[2] Lucas Parker [ID],[7,2] Matthew A. Petroff [ID],[2]
Rodrigo Reeves [ID],[8] Gary Rhoades,[2] Karwan Rostem [ID],[1] Deniz A. N. Valle [ID],[2] Duncan J. Watts [ID],[9,2]
Janet L. Weiland [ID],[2] Edward J. Wollack [ID],[1] and Zhilei Xu (徐智磊) [ID][10,2]

[1] NASA Goddard Space Flight Center, 8800 Greenbelt Road, Greenbelt, MD 20771, USA
[2] Department of Physics and Astronomy, Johns Hopkins University, 3701 San Martin Drive, Baltimore, MD 21218, USA
[3] Department of Physics, University of California, Berkeley, CA 94720, USA
[4] Facultad de Ingeniería, Universidad Católica de la Santísima Concepción, Alonso de Ribera 2850, Concepción, Chile
[5] Department of Physics, Villanova University, 800 Lancaster Avenue, Villanova, PA 19085, USA
[6] Department of Astronomy and Astrophysics, University of Chicago, 5640 South Ellis Avenue, Chicago, IL 60637, USA
[7] Space and Remote Sensing, MS D436, Los Alamos National Laboratory, Los Alamos, NM 87544, USA
[8] CePIA, Departamento de Astronomía, Universidad de Concepción, Concepción, Chile
[9] Institute of Theoretical Astrophysics, University of Oslo, P.O. Box 1029 Blindern, N-0315 Oslo, Norway
[10] MIT Kavli Institute, Massachusetts Institute of Technology, 77 Massachusetts Avenue, Cambridge, MA 02139, USA

ABSTRACT

Using the Cosmology Large Angular Scale Surveyor, we measure the disk-averaged absolute Venus brightness temperature to be 432.3 ± 2.8 K and 355.6 ± 1.3 K in the Q and W frequency bands centered at 38.8 and 93.7 GHz, respectively. At both frequency bands, these are the most precise measurements to date. Furthermore, we observe no phase dependence of the measured temperature in either band. Our measurements are consistent with a CO_2-dominant atmospheric model that includes trace amounts of additional absorbers like SO_2 and H_2SO_4.

Unified Astronomy Thesaurus concepts: Venus (1763); Brightness temperature (182); Atmospheric composition (2120)

1. INTRODUCTION

Microwave observations of Venus can be used to probe its hot and dense atmosphere that mostly ($\sim 96\%$) consists of CO_2 (Oyama et al. 1979). The greenhouse effect from the thick Venusian atmosphere, which reaches ~ 90 bars at the surface, maintains the surface temperature at ~ 750 K (Muhleman et al. 1979). While radio wavelengths $\gtrsim 4$ cm probe the surface, decreasing wavelengths successively probe increasing altitudes in the atmosphere with a steep decrease in temperature

(de Pater 1990; Butler et al. 2001). The measurement of the brightness temperature and its phase dependence at different microwave frequencies can therefore reveal important information about the composition and dynamics of various layers of the Venusian atmosphere (Pollack & Sagan 1965; Muhleman et al. 1979; de Pater et al. 1991). In this paper, we present microwave observations of Venus in the frequency bands centered near 40 and 90 GHz, corresponding to the altitudes of emission of approximately 35 and 50 km from the surface, respectively (Muhleman et al. 1979). The measurements were performed using the Cosmology Large Angular Scale Surveyor (CLASS), a telescope array located at 22°58′ S

Corresponding author: Sumit Dahal
sumit.dahal@nasa.gov

latitude and $67°47'$ W longitude in the Atacama Desert of northern Chile.

CLASS is a multifrequency polarimeter that surveys $\sim 70\%$ of the microwave sky at large angular scales with the aim of measuring the primordial gravitational wave background and constraining the optical depth due to cosmic reionization (Essinger-Hileman et al. 2014; Harrington et al. 2016). While CLASS is primarily designed to observe the cosmic microwave background (CMB) polarization, its high sensitivity allows it to observe other microwave sources within its survey area. In addition to its nominal CMB survey mode, CLASS periodically observes on-sky calibration sources including the Moon, Venus, and Jupiter to obtain telescope pointing information, characterize the beam response (Xu et al. 2020), and calibrate the detector power response to the antenna temperature of the source (Appel et al. 2019). Between 25 August 2018 and 11 October 2018, the CLASS 40 GHz (Q band) and 90 GHz (W band) telescopes performed 74 dedicated Venus observations. The same instruments observed Jupiter 70 times between 26 June 2020 and 6 August 2020. In this paper, we use Jupiter as a calibration source to constrain the brightness temperature of Venus. We also examine the phase dependence of the measured Venus brightness temperature throughout the observing campaign. We describe the observations and results in Section 2, followed by the implications of the results in Section 3.

2. OBSERVATIONS

During dedicated planet observations, we scan the telescope across the source over a small range ($\pm14°$) of azimuth angle at a fixed elevation of $45°$ while the source rises or sets through the telescope field of view ($\sim 10°$ in radius). As the telescope scans across the source, we obtain time-ordered data (TOD) for each detector at ~ 200 samples per second. During analysis, the raw TOD is first calibrated to measured optical power and then combined with the telescope pointing information to produce source-centered maps in telescope coordinates. Refer to Appel et al. (2019) and Xu et al. (2020) for further details on CLASS data acquisition, calibration from raw detector data to observed optical power, and map-making from dedicated observations.

Given the telescope beam sizes (FWHM of $\sim 1.5°$ for Q band and $\sim 0.6°$ for W band), both Venus and Jupiter ($\lesssim 1'$ in angular diameter) are well approximated as point sources for both CLASS instruments. A point source's brightness temperature (T_s) relates to the peak response as measured above the atmosphere by CLASS detectors (T_m^*) as:

$$T_s \Omega_s = T_m^* \Omega_B, \qquad (1)$$

where Ω_B is the beam solid angle and Ω_s is the solid angle subtended by the source (Page et al. 2003). To obtain T_m^* for W-band detectors, we correct the actual measured response T_m for atmospheric transmission to account for the effect of precipitable water vapor (PWV) at the CLASS site. For each observation, we obtained PWV data from the Atacama Pathfinder Experiment/the Atacama Cosmology Telescope (APEX/ACT)[1] and used the Atacama Large Millimeter/submillimeter Array atmospheric transmission model[2] based on the ATM code described in Pardo et al. (2001) to calculate the transmission correction factor for each detector. At W band, this correction was necessary because T_m^* is greater than T_m by up to $\sim 5\%$ for observations with high (~ 5 mm) PWV. However, at Q band, the effect of PWV on the derived brightness temperature ratio (Section 2.1) for a detector is $\lesssim 1\%$, which is within our measurement uncertainty; therefore no PWV-related correction was applied, i.e., $T_m^* = T_m$.

To increase the signal-to-noise ratio of the measurement, we average the source-centered maps from individual observations to form an aggregate map of the source per detector. Since Ω_s changes between observations, the averaging is done relative to a fiducial solid angle Ω_{ref}. This is achieved by scaling T_m^* from each observation by a factor of Ω_{ref}/Ω_s while averaging the maps. To determine Ω_s subtended by a planet, we use the distance to the planet that varies for each observation and a fixed disk radius (R). For Jupiter, we calculate an effective R for the projected area of its oblate disk using the method described in Weiland et al. (2011). For Venus, we use a standard disk radius of 6120 km (Muhleman et al. 1979; Fahd & Steffes 1992; Butler et al. 2001), which includes the physical surface radius of Venus (~ 6052 km) plus the height of the atmosphere. This choice of Venus disk radius allows our results to be compared with previous measurements and the brightness temperature models presented in Section 3.

2.1. *Brightness Temperature*

For averaged planet maps, we can write Equation 1 as $T_s\Omega_{ref} = T_{ref}\Omega_B$, where T_{ref} is the average of ($T_m^* \times \Omega_{ref}/\Omega_s$) values acquired over the observing campaign for a particular detector. We set Ω_{ref} to be the same for both Venus and Jupiter per-detector averaged

---
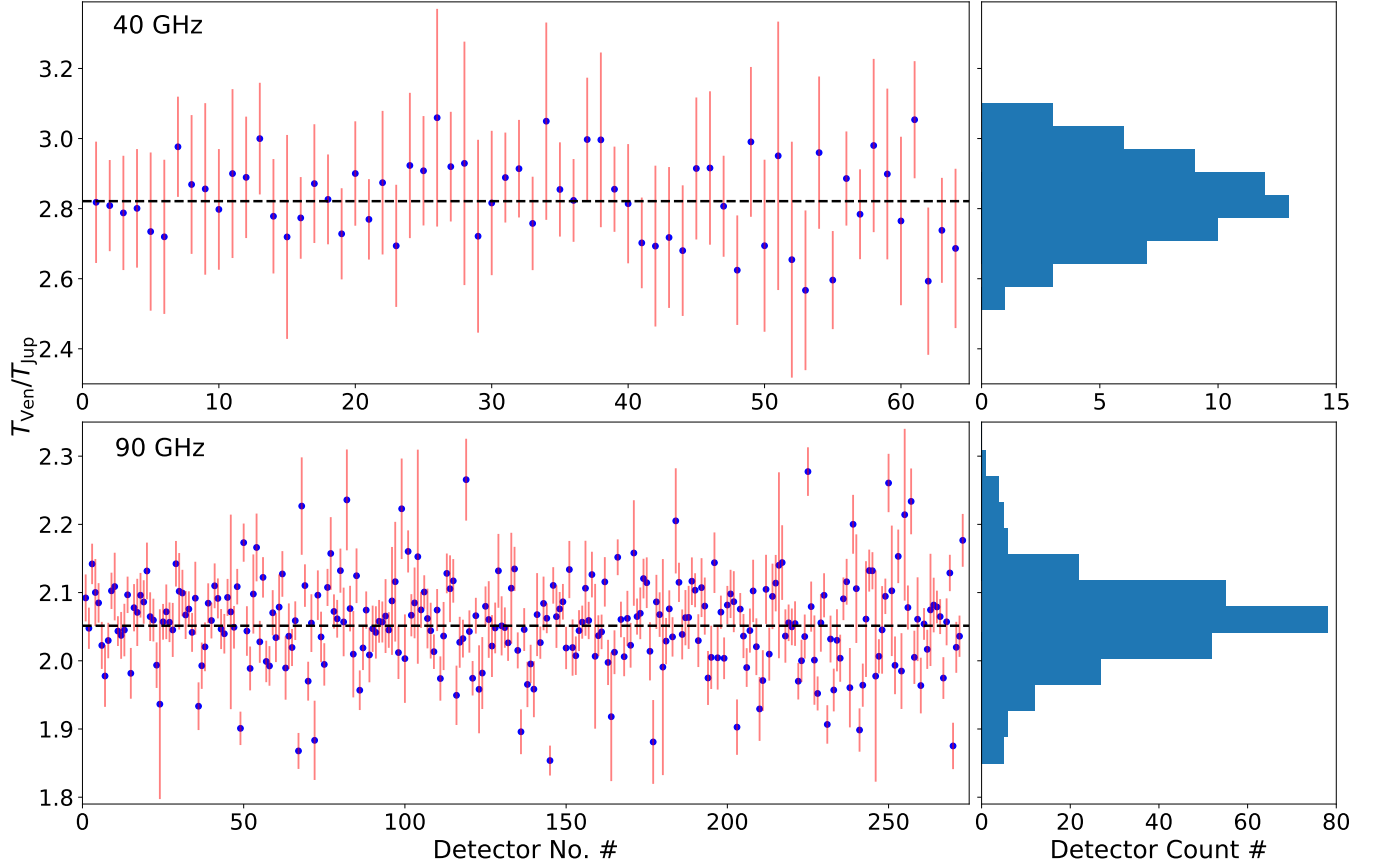
Figure 1. (Left) Venus-to-Jupiter brightness temperature ratios measured by the CLASS 40 and 90 GHz detectors. Each data point corresponds to the result obtained from the averaged maps for a particular detector. For a given detector, the brightness temperature ratio was calculated by taking the ratio of measured peak amplitudes of Venus and Jupiter, both scaled to the same fiducial reference solid angle of 5.5×10^{-8} sr. The errors in the ratios are the combined errors from the Venus and Jupiter amplitude measurements, which were calculated from the variance of baseline measurements away from the source. The inverse-variance weighted mean ratios (dashed lines) for the 40 and 90 GHz detectors are 2.821 ± 0.015 and 2.051 ± 0.004, respectively. (Right) Corresponding histograms of the brightness temperature ratio measurements.

maps so that the ratio of peak responses measured by CLASS detectors $T_{\rm ref}({\rm Ven})/T_{\rm ref}({\rm Jup})$ is equal to the ratio of brightness temperatures $T_{\rm Ven}/T_{\rm Jup}$. We calculated $T_{\rm ref}({\rm Ven})$ and $T_{\rm ref}({\rm Jup})$ values for $\Omega_{\rm ref} = 5.5 \times 10^{-8}$ sr (i.e., $54.55''$ diameter) to obtain the $T_{\rm Ven}/T_{\rm Jup}$ ratios shown in Figure 1. For 40 GHz (90 GHz), out of 71 (331) detectors that detected both Venus and Jupiter, we consider 64 (273) of them with $T_{\rm Ven}/T_{\rm Jup}$ between 2.5 and 3.2 (1.8 and 2.4) and uncertainty in the ratio $< 15\%$ (10%) for this analysis. These particular choices of data filters were applied to reject the detectors that were affected by excess noise or improper calibration from raw TOD to optical power. The uncertainties in the ratios shown in Figure 1 are the combined errors from the Venus and Jupiter peak amplitude (in units of optical power) measurements, which were obtained from the variance of baseline measurements away from the source and include the calibration error from raw TOD

to optical power. With about 5% calibration error per measurement (J. W. Appel et al. 2021, in preparation) and ~ 50 maps averaged per detector, the contribution from statistical calibration error is $\sim 0.7\%$ of the measured amplitude.

For the 40 and the 90 GHz detector arrays, the inverse-variance weighted mean $T_{\rm Ven}/T_{\rm Jup}$ ratios are 2.821 ± 0.015 and 2.051 ± 0.004, respectively, where the uncertainties are the standard errors on the mean. Using bootstrapping, we verified that these standard errors represent the uncertainties in the mean of the underlying distributions. For both frequency bands, the standard deviation of the mean values of 10^6 bootstrap-generated resamples (the statistic converges well before 10^6 resamplings) is same as the standard error of the parent sample.

To obtain Venus brightness temperatures, we multiply these CLASS-measured mean $T_{\rm Ven}/T_{\rm Jup}$ ratios by

T_{Jup} values from the Wilkinson Microwave Anisotropy Probe (WMAP), calibrated with respect to the CMB dipole. Bennett et al. (2013) reported nine-year mean T_{Jup} values of 154.3 ± 0.59 K and 172.8 ± 0.52 K at Q and W bands centered at 40.78 ± 0.07 GHz and 93.32 ± 0.19 GHz, respectively. The effective Rayleigh-Jeans (RJ) point source center frequencies for CLASS Q and W band detectors are 38.8 ± 0.2 GHz and 93.7 ± 0.2 GHz, respectively (S. Dahal et al. 2021, in preparation). To correct for the difference in effective center frequencies between CLASS and WMAP detectors at Q band, we utilize two different methods to compute T_{Jup} at 38.8 GHz: (1) a local power law fit between WMAP's Ka and Q band measurements gives $T_{\mathrm{Jup}} = 152.56 \pm 0.61$ K, and (2) the nominal Radio BErkeley Atmospheric Radiative transfer (RadioBEAR)[3] model provides T_{Jup} of 152.58 K. We adopt our local power law fit to the WMAP T_{Jup} spectrum for further analysis, since although the RadioBEAR model agrees well with the WMAP measurements at Q and V bands, the model is $\sim 0.7\%$ higher at Ka band. It is notable that the close proximity of the CLASS and WMAP Q-band center frequencies results in agreement between the two methods at 38.8 GHz. At W band, since the CLASS and WMAP effective center frequencies are close with overlapping error bars, the frequency correction is not necessary. Combined with the CLASS-measured mean $T_{\mathrm{Ven}}/T_{\mathrm{Jup}}$ ratios, these T_{Jup} values yield the Venus brightness temperature of 430.4 ± 2.8 K at Q band and 354.5 ± 1.3 K at W band.

These brightness temperature values are measured with respect to blank sky; they do not include the CMB contribution blocked by the planet, which is included in the background. Therefore, to get the absolute RJ brightness temperature of Venus, we add the RJ temperature of the CMB: 1.9 K at Q band and 1.1 K at W band (Fixsen et al. 1996; Page et al. 2003). As a result, we get the absolute Venus brightness temperature of 432.3 ± 2.8 K and 355.6 ± 1.3 K at Q and W bands, respectively. To our knowledge, these results are the most precise disk-averaged Venus brightness temperature measurements to date at both frequency bands.

2.2. Phase

During the CLASS Venus observing campaign, the solar illumination of Venus changed from 44% to 8% (with 100% illumination occurring at superior conjunction). To examine the phase dependence of the Venus brightness temperature, we calculate the detector array-

[3] https://github.com/david-deboer/radiobear
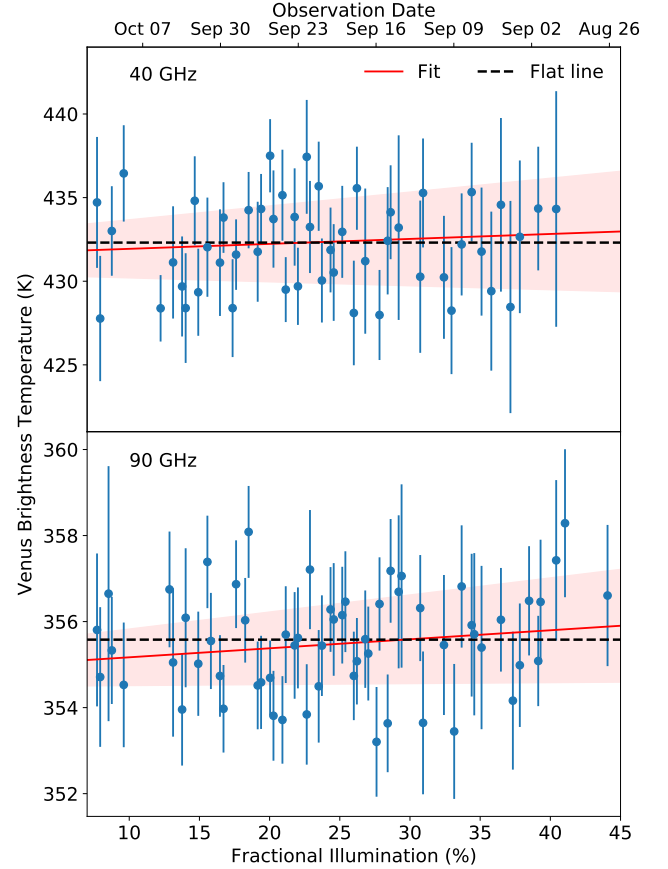
Figure 2. Measured brightness temperature versus fractional solar illumination (phase) of Venus during the observing campaign. Each data point corresponds to the detector array-averaged temperature value for that particular day. While, over time, the fractional illumination decreases from 44% to 8%, we do not observe any statistically significant phase dependence of the measured temperatures. The best fit lines (solid red) correspond to a gradient of 0.03 ± 0.05 K/% and 0.02 ± 0.02 K/% for the 40 and the 90 GHz observations, respectively. The shaded regions show 1σ uncertainties for the fits. For comparison, the flat dashed lines show the absolute brightness temperature values calculated in Section 2.1.

averaged temperature values for individual observations (i.e., before averaging the maps) using the Jupiter-based calibration discussed in Section 2.1. As discussed earlier in this section, the individual W-band measurements have been corrected for the effect of PWV. Figure 2 shows the array-averaged Venus brightness temperature values plotted against the fractional solar illumination and its corresponding observation date. During this observing period, we detect no phase dependence of the Venus brightness temperature; the gradient of the array-averaged temperature values for different solar illuminations is statistically consistent with a flat line for both

frequency bands. The best fit lines have gradients of 0.03 ± 0.05 K/% and 0.02 ± 0.02 K/% for the 40 and the 90 GHz frequency bands, respectively.

3. DISCUSSION

The microwave thermal emission from Venus is strongly affected by its atmospheric opacity. Venusian atmospheric models (de Pater et al. 1991; Fahd & Steffes 1992) predict that the opacity provided by CO_2 alone leads to brightness temperatures of 444 K and 367 K at 40 and 90 GHz frequencies, respectively. Any presence of additional absorbers like SO_2 and H_2SO_4 increases the opacity of Venus at these frequencies. This moves the radiative transfer weighting function higher in the atmosphere to colder altitudes (de Pater et al. 1991), hence decreasing the predicted brightness temperature. In Figure 3, we compare our measurements to three different Venusian brightness temperature models: (1) CO_2 only, (2) CO_2 with SO_2 models from Fahd & Steffes (1992), and (3) CO_2 with both SO_2 and H_2SO_4 (gaseous) from Akins & Steffes (2020). In the second model, the abundance profile for SO_2 is set to 62 ppm below 48 km altitude (the lower cloud base) and exponentially decreasing above 48 km. For the third model with both additional components, a uniform subcloud SO_2 abundance of 50 ppm along with an H_2SO_4 abundance ranging from 10–14 ppm following the equatorial profile from Kolodner & Steffes (1998) is used. While the temperature and pressure profiles used in all three models are based on probe measurements over low Venusian latitudes, we note that the difference between the models with and without H_2SO_4 could be partly attributed to the difference in assumed profiles. Refer to Fahd & Steffes (1992) and Akins & Steffes (2020) for further details on these models.

At both frequency bands, our measurements agree with a CO_2-dominant atmospheric model. Furthermore, given their precision, our measured brightness temperature values favor the presence of trace amounts of additional absorbers. As shown in Figure 3, our measured brightness temperature is consistent with the H_2SO_4 model at Q band and prefers a slightly lower H_2SO_4 abundance at higher altitudes probed by W-band frequencies. Our data also supports a CO_2+SO_2 model with SO_2 concentration slightly higher than 62 ppm. However, identifying the exact content and abundance of these additional absorbers requires further modeling of the Venusian atmosphere and is outside the scope of this work. We also note that the CO_2-only model from Fahd & Steffes (1992) is inconsistent ($> 5\sigma$) with our measurements at both frequencies. In Figure 3, we also compare our values with two previous measurements in
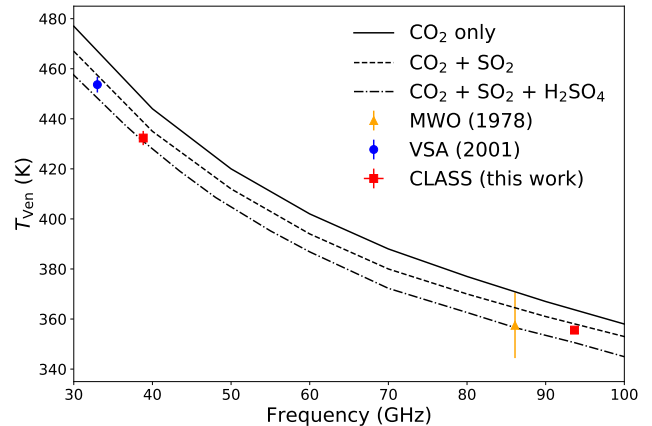
Figure 3. Microwave spectrum of Venus. We compare the CLASS measurements with previous measurements from the Millimeter Wave Observatory (MWO; Ulich et al. 1980) at W band and the Very Small Array (VSA; Hafez et al. 2008) at Ka band. We also plot three different brightness temperature models: CO_2 only (solid) and CO_2+SO_2 (dashed) from Fahd & Steffes (1992), and $CO_2+SO_2+H_2SO_4$ (dashed-dotted) from Akins & Steffes (2020). In the CO_2+SO_2 model, the SO_2 abundance is set to 62 ppm below the cloud base and exponentially decreasing above it. For the model with H_2SO_4, the sub-cloud SO_2 abundance is set to 50 ppm whereas the gaseous H_2SO_4 abundance ranges from 10–14 ppm following the equatorial profile presented in Kolodner & Steffes (1998). CLASS measurements are inconsistent with the CO_2-only model and prefer the presence of trace amounts of additional absorbers at both frequency bands.

this frequency range. Our brightness temperature values are consistent with the Ulich et al. (1980) measurement at 86.1 GHz and the Hafez et al. (2008)[4] measurement at 33 GHz.

The lack of phase dependence in our measured brightness temperatures is also in agreement with the insignificant temperature variation throughout 1.5 synodic cycles of Venus reported by Hafez et al. (2008). Previously, Basharinov et al. (1965) reported $T_{\rm Ven} = 427 + 41\cos(\Phi - 21°)$ K, where $-180° < \Phi < 180°$ is the Venus phase angle, based on their 37.5 GHz observations near superior conjunction ($\Phi = 0°$). To explain this observation, Pollack & Sagan (1965) used an atmospheric model with dust distributed through the lower atmosphere with preferential abundance in the illuminated hemisphere, which could lead to

---

[4] Hafez et al. (2008) reported $T_{\rm Ven} = 460.3 \pm 3.2$ K relative to blank sky, $T_{\rm Jup} = 146.6$ K, and Venus angular size based on its surface radius. We use an updated $T_{\rm Jup} = 147.1$ K from Bennett et al. (2013) and correct for the standard Venus disk radius and CMB contribution to obtain the final absolute $T_{\rm Ven} = 453.6 \pm 3.1$ K.

the approximately 10% variation in the Q-band brightness temperature amplitude relative to the Venus phase. This is inconsistent with both the Hafez et al. (2008) observations and the results presented in this paper. Our measured brightness temperature at Q band, which agrees with the CO_2-dominant atmospheric model (Figure 3), also does not require the dust-filled model from Pollack & Sagan (1965). The lack of phase dependence at Q band may suggest strong enough winds in the CO_2-dominant lower atmospheric layers to evenly distribute the temperature around the planet. This would also explain the lack of phase dependence we observe at W band. However, pinpointing the exact mechanism behind the lack of phase dependence at these microwave frequencies requires further investigation.

Both CLASS Q- and W-band telescopes continue to observe the microwave sky from the Atacama Desert in Chile. Future data from these instruments will provide improved phase coverage of the Venusian illumination, which can help further characterize the phase-dependent temperature variation (if any) at these microwave frequencies. Furthermore, CLASS has started observations with a dichroic instrument (Dahal et al. 2020) operating at frequency bands centered near 150 and 220 GHz. The addition of this high-frequency data will also improve our frequency coverage in the Venus spectrum, providing better understanding of the Venusian atmosphere.

4. SUMMARY

We present Venus observations performed with the Q-band and the W-band CLASS telescopes. Using Jupiter as a calibration source, we measure the disk-averaged absolute brightness temperature of Venus to be 432.3 ± 2.8 K and 355.6 ± 1.3 K in the Q and W bands centered at 38.8 ± 0.2 GHz and 93.7 ± 0.2 GHz, respectively. These results are the most precise Venus brightness temperature measurements to date. At both frequency bands, the measured brightness temperature values are consistent with CO_2-dominant atmospheric models (de Pater et al. 1991; Fahd & Steffes 1992; Akins & Steffes 2020) and previous measurements from Ulich et al. (1980) and Hafez et al. (2008). During our two-month observing campaign, while the fractional solar illumination of Venus changed from 44% to 8%, we did not observe any phase dependence of the brightness temperature in either frequency band. This lack of phase dependence agrees with the measurement from Hafez et al.

(2008) and does not support the brightness temperature versus phase relation at Q band reported by Basharinov et al. (1965).

REFERENCES

Akins, A. B., & Steffes, P. G. 2020, Icarus, 351, 113928, doi: 10.1016/j.icarus.2020.113928

Appel, J. W., Xu, Z., Padilla, I. L., et al. 2019, ApJ, 876, 126, doi: 10.3847/1538-4357/ab1652

Astropy Collaboration, Robitaille, T. P., Tollerud, E. J., et al. 2013, A&A, 558, A33, doi: 10.1051/0004-6361/201322068

Basharinov, A. E., Vetukhnovskaya, Y. N., Kuz'min, A. D., Kutuza, B. G., & Salomonovich, A. E. 1965, Soviet Ast., 8, 563

Bennett, C. L., Larson, D., Weiland, J. L., et al. 2013, ApJS, 208, 20, doi: 10.1088/0067-0049/208/2/20

Bustos, R., Rubio, M., Otárola, A., & Nagar, N. 2014, PASP, 126, 1126, doi: 10.1086/679330

Butler, B. J., Steffes, P. G., Suleiman, S. H., Kolodner, M. A., & Jenkins, J. M. 2001, Icarus, 154, 226, doi: 10.1006/icar.2001.6710

Dahal, S., Amiri, M., Appel, J. W., et al. 2020, Journal of Low Temperature Physics, 199, 289, doi: 10.1007/s10909-019-02317-0

de Pater, I. 1990, ARA&A, 28, 347, doi: 10.1146/annurev.aa.28.090190.002023

de Pater, I., Sault, R. J., Wong, M. H., et al. 2019, Icarus, 322, 168, doi: 10.1016/j.icarus.2018.11.024

de Pater, I., Schloerb, F., & Rudolph, A. 1991, Icarus, 90, 282 , doi: https://doi.org/10.1016/0019-1035(91)90107-5

de Pater, I., Fletcher, L. N., Luszcz-Cook, S., et al. 2014, Icarus, 237, 211, doi: 10.1016/j.icarus.2014.02.030

Essinger-Hileman, T., Ali, A., Amiri, M., et al. 2014, Society of Photo-Optical Instrumentation Engineers (SPIE) Conference Series, Vol. 9153, CLASS: the cosmology large angular scale surveyor, 91531I, doi: 10.1117/12.2056701

Fahd, A. K., & Steffes, P. G. 1992, Study and interpretation of the millimeter-wave spectrum of Venus, Technical Report No. 1992-1, Georgia Institute of Technology Final Report

Fixsen, D. J., Cheng, E. S., Gales, J. M., et al. 1996, ApJ, 473, 576, doi: 10.1086/178173

Hafez, Y. A., Davies, R. D., Davis, R. J., et al. 2008, MNRAS, 388, 1775, doi: 10.1111/j.1365-2966.2008.13515.x

Harrington, K., Marriage, T., Ali, A., et al. 2016, Society of Photo-Optical Instrumentation Engineers (SPIE) Conference Series, Vol. 9914, The Cosmology Large Angular Scale Surveyor, 99141K, doi: 10.1117/12.2233125

Hunter, J. D. 2007, Computing in Science Engineering, 9, 90, doi: 10.1109/MCSE.2007.55

Kolodner, M. A., & Steffes, P. G. 1998, Icarus, 132, 151, doi: 10.1006/icar.1997.5887

Muhleman, D. O., Orton, G. S., & Berge, G. L. 1979, ApJ, 234, 733, doi: 10.1086/157550

Oyama, V. I., Carle, G. C., Woeller, F., & Pollack, J. B. 1979, Science, 203, 802, doi: 10.1126/science.203.4382.802

Page, L., Barnes, C., Hinshaw, G., et al. 2003, ApJS, 148, 39, doi: 10.1086/377223

Pardo, J. R., Cernicharo, J., & Serabyn, E. 2001, IEEE Transactions on Antennas and Propagation, 49, 1683, doi: 10.1109/8.982447

Pollack, J. B., & Sagan, C. 1965, Icarus, 4, 62 , doi: https://doi.org/10.1016/0019-1035(65)90018-7

Rhodes, B. C. 2011, PyEphem: Astronomical Ephemeris for Python. http://ascl.net/1112.014

Ulich, B., Davis, J., Rhodes, P., & Hollis, J. 1980, IEEE Transactions on Antennas and Propagation, 28, 367, doi: 10.1109/TAP.1980.1142330

van der Walt, S., Colbert, S. C., & Varoquaux, G. 2011, Computing in Science Engineering, 13, 22, doi: 10.1109/MCSE.2011.37

Virtanen, P., Gommers, R., Oliphant, T. E., et al. 2020, Nature Methods, 17, 261, doi: 10.1038/s41592-019-0686-2

Weiland, J. L., Odegard, N., Hill, R. S., et al. 2011, ApJS, 192, 19, doi: 10.1088/0067-0049/192/2/19

Xu, Z., Brewer, M. K., Rojas, P. F., et al. 2020, The Astrophysical Journal, 891, 134, doi: 10.3847/1538-4357/ab76c2